

Easier said than done: unexpected hurdles to preparing ~1,000 cranial CT scans for data collection from an online digital repository

Mario Modesto-Mata Corresp., 1, 2, Arthur Thiebaut 1, Kristin L Krueger 3, A. Murat Maga 4, Jessica L Joganic 5, Timothy M Ryan 6, Joan T Richtsmeier 6, James M Cheverud 7, Leslea J Hlusko Corresp. 1

Corresponding Authors: Mario Modesto-Mata, Leslea J Hlusko Email address: paleomariomm@gmail.com, leslea.hlusko@cenieh.es

Background. As science becomes more open and accessible, researchers are increasingly encouraged—and sometimes required—to share their digital data on public repositories. While this promotes transparency and reusability, it can also introduce challenges. We highlight one such challenge by detailing our experience processing CT scans of 985 baboon skulls downloaded from MorphoSource, part of a quantitative genetic study of craniodental variation in the pedigreed baboon colony from the Southwest National Primate Research Center. When importing DICOM files into 3D Slicer, 182 of the 985 scans (18.5%) generated an "inconsistent slice spacing" error. When prompted, 3D Slicer "corrected" this by regularizing the slice spacing. However, this led to a mismatch between the slice spacing reported on MorphoSource and the spacing adjusted by 3D Slicer.

Methods. To determine which slice spacing was accurate, we compared Prosthion-Basion (PR-BA) distances measured directly from physical skulls (using calipers and a Microscribe) with those derived from the CT models. Our comparison sample included 10 skulls from the error group and 20 from the error-free group.

Results. For scans without the slice spacing error, there was strong agreement between physical and digital measurements, suggesting metadata accuracy. For error-generating scans, measurements based on 3D Slicer's corrected spacing and Amira-Avizo both aligned well with the physical data. In contrast, manually overriding the spacing to match the MorphoSource metadata led to overestimations of the PR-BA distance.

Conclusion. Although the discrepancy was straightforward to describe, resolving it required over 250 person-hours across 8 months. Accessing physical specimens, conducting repeated measurements, and cross-validating with multiple tools made the process labor-intensive. Nonetheless, this effort avoided a 3–5% measurement bias in nearly 20% of our sample and allowed inclusion of these scans in downstream semi-automated data collection. We urge researchers to thoroughly understand the digital datasets they work with and resist the temptation to ignore apparent errors during import. We also recommend that funding bodies provide support for the extensive time needed to validate and process digital imagery, Peerl reviewing PDF | (2025:03:119166:1:1:NEW 13 Aug 2025)

¹ Centro Nacional de Investigación sobre la Evolución Humana, Burgos, Castilla y León, Spain

² Universidad Internacional de La Rioja, Logroño, La Rioja, Spain

³ Department of Anthropology, Loyola University of Chicago, Chicago, Illinois, United States

⁴ Department of Pediatrics, University of Washington School of Medicine, Seattle, Washington, United States

National Park Service, Ashland, Wisconsin, United States

⁶ Department of Anthropology, Pennsylvania State University, University Park, Pennsylvania, United States

⁷ Department of Biology, Loyola University of Chicago, Chicago, Illinois, United States



both for data generators and users. Finally, we highlight the need for public repositories to implement stronger quality control. If a data import check similar to 3D Slicer's had been applied during data submission, the inconsistency between manually entered metadata and embedded DICOM information might have been caught and corrected at the time of upload.



Easier said than done: unexpected hurdles to preparing ~1,000 cranial CT scans for data collection from an online digital repository

4	
4 5	Mario Modesto-Mata ^{1,2} , Arthur Thiebaut ¹ , Kristin L. Krueger ³ , A. Murat Maga ⁴ , Jessica L. Joganic ⁵ , Timothy M. Ryan ⁶ , Joan T. Richtsmeier ⁶ , James M. Cheverud ⁷ , Leslea J. Hlusko ¹
6	
7 8	¹ Centro Nacional de Investigación sobre la Evolución Humana (CENIEH), Burgos, (Castilla y León, Spain)
9	² Universidad Internacional de La Rioja (UNIR), Logroño (La Rioja, Spain)
LO	³ Department of Anthropology, Loyola University Chicago, USA
l1 l2	⁴ Department of Pediatrics, University of Washington School of Medicine, Seattle, Washington, USA
13	⁵ National Park Service, , Ashland, Wisconsin, USA
L4 L5	⁶ Department of Anthropology, Pennsylvania State University, University Park, Pennsylvania, USA
16	⁷ Department of Biology, Loyola University Chicago, USA
7	
18	Corresponding authors:
19	Mario Modesto-Mata ^{1,2}
20 21	Centro Nacional de Investigación sobre la Evolución Humana (CENIEH), Paseo Sierra de Atapuerca 3, 09002 Burgos, Spain
22	Universidad Internacional de La Rioja (UNIR), Av. de la Paz 137, 26006 Logroño (La Rioja,
23	Spain)
24	Email address: paleomariomm@gmail.com
25	
26	Leslea J. Hlusko ¹
27	Centro Nacional de Investigación sobre la Evolución Humana (CENIEH), Paseo Sierra de
28	Atapuerca 3, 09002 Burgos, Spain
29	Email address: <u>leslea.hlusko@cenieh.es</u>



Abstract

- 32 **Background.** As science becomes more open and accessible, researchers are increasingly
- 33 encouraged—and sometimes required—to share their digital data on public repositories. While
- 34 this promotes transparency and reusability, it can also introduce challenges. We highlight one
- 35 such challenge by detailing our experience processing CT scans of 985 baboon skulls
- 36 downloaded from MorphoSource, part of a quantitative genetic study of craniodental variation in
- 37 the pedigreed baboon colony from the Southwest National Primate Research Center. When
- 38 importing DICOM files into 3D Slicer, 182 of the 985 scans (18.5%) generated an "inconsistent
- 39 slice spacing" error. When prompted, 3D Slicer "corrected" this by regularizing the slice spacing.
- 40 However, this led to a mismatch between the slice spacing reported on MorphoSource and the
- 41 spacing adjusted by 3D Slicer.
- 42 **Methods.** To determine which slice spacing was accurate, we compared Prosthion-Basion (PR-
- 43 BA) distances measured directly from physical skulls (using calipers and a Microscribe) with
- 44 those derived from the CT models. Our comparison sample included 10 skulls from the error
- 45 group and 20 from the error-free group.
- 46 **Results.** For scans without the slice spacing error, there was strong agreement between physical
- 47 and digital measurements, suggesting metadata accuracy. For error-generating scans,
- 48 measurements based on 3D Slicer's corrected spacing and Amira-Avizo both aligned well with
- 49 the physical data. In contrast, manually overriding the spacing to match the MorphoSource
- 50 metadata led to overestimations of the PR-BA distance.
- 51 **Conclusion.** Although the discrepancy was straightforward to describe, resolving it required over
- 52 250 person-hours across 8 months. Accessing physical specimens, conducting repeated
- 53 measurements, and cross-validating with multiple tools made the process labor-intensive.
- Nonetheless, this effort avoided a 3–5% measurement bias in nearly 20% of our sample and
- 55 allowed inclusion of these scans in downstream semi-automated data collection. We urge
- researchers to thoroughly understand the digital datasets they work with and resist the temptation
- 57 to ignore apparent errors during import. We also recommend that funding bodies provide support
- 58 for the extensive time needed to validate and process digital imagery, both for data generators and
- 59 users. Finally, we highlight the need for public repositories to implement stronger quality control.
- 60 If a data import check similar to 3D Slicer's had been applied during data submission, the
- 61 inconsistency between manually entered metadata and embedded DICOM information might
- have been caught and corrected at the time of upload.

64 Introduction

- 65 Development of digital specimen repositories has significantly advanced the goal of data-sharing
- and democratization of the anatomical sciences by making immense numbers of scanned
- 67 biological specimens available to any researcher with access to the internet (Weber et al., 2001;
- 68 Bradtmöller et al., 2010; Copes et al., 2016; Boyer et al., 2016; Lebrun & Orliac, 2016; Davies et



- 69 al., 2017; Blackburn et al., 2024). For example, the data aggregator iDigBio (Nelson, 2014)
- 70 enables the research community to have access to millions of biological specimens in digital
- 71 format (Nelson & Paul, 2019). Taxa available for study are incredibly diverse and include
- 72 (Singer, Love & Page, 2018), bats (Shi, Westeen & Rabosky, 2018), non-human primates (Copes
- et al., 2016; Barger et al., 2021), reptiles (Uetz et al., 2024) and humans medical imaging
- 74 (Vannier, Staab & Clarke, 2002; Clark et al., 2013; Edgar et al., 2020; Lebre, Silva & Costa,
- 75 2020). The research potential of these 3D digital repositories is immeasurable, although the use
- of images from human subjects comes with complicating ethical factors (Schug et al., 2020;
- 77 Spake, Nicholas & Cardoso, 2020).
- 78 Traditional measurement methods provide a striking contrast with the modalities available for the
- 79 analysis of these virtual models. In the past, physical specimens were measured directly or from
- 80 high-resolution analog replicas; cranial and endocranial distances and brain sizes were obtained
- 81 via physical instruments (Pickering, 1930; Wagner, 1935) or radiographs (Hansman, 1966), and
- 82 mesiodistal and buccolingual tooth diameters measured with calipers (Garrod et al., 1928; Garn,
- 83 Lewis & Kerewsky, 1966; Boklage, 1987). It was not until the final decades of the 20th century
- 84 that laser scanning in paleoanthropology made 3D models available for virtual measurements
- 85 (Zollikofer, Ponce De León & Martin, 1998), and tomographic and microtomographic techniques
- 86 (CT and mCT) transformed fossil analysis and data distribution (Sutton, 2008; Wu & Schepartz,
- 87 2009). Today, virtual reconstructions of fossils allow for the acquisition of previously
- 88 inaccessible measurements, for example, enabling researchers to calculate enamel and dentine
- 89 surfaces and volumes in fossilized dentitions (Martínez de Pinillos et al., 2017; García-Campos et
- 90 al., 2019; Martín-Francés et al., 2020), analyze the internal structures of cranial bones such as
- 91 diploic channels (Lázaro et al., 2020), and explore the auditory capacities of ancient taxa through
- 92 cochlear studies (Conde-Valverde et al., 2019), just to name a few. Additionally, virtual models
- 93 support the broad application of new statistical methods, including geometric morphometrics
- 94 (Bruner, 2004; Bastir et al., 2017; Palancar et al., 2021) and artificial intelligence techniques (Yu
- 95 et al., 2022, 2024).
- 96 When uploading for open-source, resources are available for guidance on how to prepare image
- 97 files prior to upload and advice on how to follow the F.A.I.R. principles: Findable, Accessible,
- 98 Interoperable, and Reusable (Wilkinson et al., 2016; Davies et al., 2017; Jacobsen et al., 2020).
- 99 Additionally, there are resources that guide investigators on how to utilize CT scans downloaded
- from these repositories (Buser et al., 2020), urge caution with respect to the sources of 3D
- measurement error (Shearer et al., 2017), and provide warnings about compiling 3D data from
- other researchers (Robinson & Terhune, 2017). However, in our review of the literature, we were
- 103 unable to find scientific publications specifically aimed at providing perspective on the time
- investment needed to prepare data prior to making them publicly available, or shedding light on
- the challenges and time investment that researchers may need to prepare 3D scans from these
- 106 data repositories.
- Here, we share our experience preparing 985 CT scans of baboon crania downloaded from a
- public image repository for data collection. These scans derive from one population of baboons
- that is part of a pedigreed breeding colony at the Southwest National Primate Research Center



- (SNPRC), a colony that has been used in quantitative genetic analyses (Rogers et al., 2000; Cox
- et al., 2006) for phenotypes that include dental variation (Hlusko et al., 2004, 2016), craniofacial
- variation (Sherwood et al., 2008; Willmore et al., 2009; Roseman et al., 2010; Joganic et al.,
- 2018), cardiovascular disease (Mahaney et al., 2018), bone density (Havill et al., 2010), life span
- 114 (Martin et al., 2002), and even dimensions of personality (Johnson et al., 2015). Additionaly,
- these baboons have been widely used to answer research questions about genomics (Spradling et
- al., 2013; Robinson et al., 2019; Kos et al., 2021), pathology (Szabó & Salinas, 2021),
- microbiology (Tsukayama et al., 2018), and brain architecture (Atkinson et al., 2015).
- 118 Given the large sample size needed for quantitative genetic analyses, we planned to automate
- parts of the phenotype data collection process to save time (Boukamcha et al., 2017; Bannister et
- al., 2020; Kang et al., 2021; Nguyen et al., 2022). Recently, a new pipeline has been developed
- using automatic landmarking via multiple templates (MALPACA) (Zhang et al., 2022). The
- process is deployed as a module in the Slicermorph extension (Rolfe et al., 2021) that runs in 3D
- 123 Slicer (Fedorov et al., 2012) and has been used successfully to analyze zebrafish models
- 124 (Diamond et al., 2023). In preparation of the 985 SNPRC CT scans for use with MALPACA, we
- 125 first imported the DICOM files to 3D Slicer. It was during this step that we ran into a hurdle that
- required an unexpected and extended investment in time.
- We present our journey in this article for four primary reasons. First, we want to provide the
- solution, which required access to physical specimens, so that future users of these CT scans will
- know how to modify the files accordingly. Second, our experience can serve as a cautionary tale
- 130 for others when they are anticipating the amount of time that may be needed to prepare CT scans
- for data collection. Third, a warning for future researchers to thoroughly understand their digital
- datasets and question every potential inconsistency or error. And fourth, we hope that this
- 133 situation will provide motivation for colleagues to ask funding agencies for adequate support for
- preparing and uploading their CT scans to a digital repository, as part of following the best
- practices for publishing verified 3D digital data (Davies et al., 2017).

137

138

Materials & Methods

The baboon colony and skull collection

- 139 The baboon (genus *Papio*) skeletal sample came from a colony maintained by the Southwest
- 140 National Primate Research Center (SNPRC), located at the Texas Biomedical Research Institute
- in San Antonio (Texas, USA). The founders of this colony were wild baboons caught in
- southwestern Kenya, in a hybrid area between two subspecies: olive baboons (*P. hamadryas*
- anubis) and yellow baboons (P. h. cynocephalus) (Maples & McKern, 1967), although the
- majority of founders were from the former subspecies. More than 2,400 individuals out of the
- roughly 21,000 who have resided within the SNPRC colony form a single, complex pedigree for
- which their kinship relations are well documented (Rogers et al., 2000; Hlusko, Weiss &
- 147 Mahaney, 2002; Joganic et al., 2018). Traditionally, all members of *Papio* were interpreted as one
- species, *P. hamadryas*, and the different geographic variants were considered different subspecies



166

- 149 (Jolly, 2003). This is the approach followed by the SNPRC. More recent taxonomic practice is to
- 150 divide Papio into six different species with significant hybridization between them (Boissinot et
- al., 2014). We adopt here the naming convention of the SNPRC, as in this paper the taxonomy of
- this complex genus is not the aim.
- 153 After dying, each baboon was necropsied by SNPRC veterinarians, skeletonized via maceration
- or with dermestid beetles, and their skulls archived at Washington University in St. Louis
- 155 (WUSTL) under the curation of JMC and J.L.J. While residing at the SNPRC, each animal was
- assigned a four-, five-, or six-digit alphanumeric identification number. During the transition
- 157 from the SNPRC to the WUSTL skeletal collection, each skull was given a new specimen
- number beginning with "W" and running from W001 to W985. These skulls were later
- transferred to Loyola University in Chicago but are now in the process of being shifted to the
- 160 University of Illinois Urbana-Champaign (to be maintained by Charles Roseman).

The cranial CT scans

- Nine hundred and eighty-five skulls were imaged using a Siemens Biograph 40 TruePoint
- 163 Tomograph at the Center for Clinical Imaging Research at Washington University School of
- Medicine. The resulting CT images were uploaded to MorphoSource between March 2018 and
- August 2019 (https://www.morphosource.org/projects/00000C475).
- 167 The term "slice thickness" reports the amount of anatomical information contained within a
- single CT image or slice. This contrasts with "slice spacing," the distance between the center of
- two consecutive DICOM slices. Slice spacing and thickness can be the same or different,
- depending on the acquisition parameters. However, the geometry of the volume (3D data) is
- determined by the slice spacing parameter. For these baboon skull CT images, these parameters
- are the same, and because the term "slice spacing" is used in 3D Slicer, this is the term that we
- 173 employ here.
- 174 According to the CT scan metadata provided on MorphoSource, individuals W001 to W487 were
- scanned at a slice spacing of 0.75 mm, and individuals W488 to W985 were scanned with a slice
- 176 spacing of 0.60 mm. Willmore et al. (2009), Roseman et al. (2010), Joganic et al. (2018), and
- Joganic & Heuzé (2019) analyzed data collected from a subset of the skulls scanned with the 0.75
- and 0.60 mm slice spacing, and their description of the scanner and scan settings agree with the
- information provided on MorphoSource. Atkinson et al. (2015, 2016) analyzed data from the full
- data set of 985 individuals but reported that the slice spacing was either 0.6 or 0.7 mm for all
- specimens (Atkinson et al., 2015), and that they used a General Electric 3D CT scanner.
- However, the metadata described by MorphoSource, and reported by Willmore et al. (2009) and
- 183 Roseman et al. (2010) indicates 0.75 mm slice spacing and that a Siemens scanner was used. We
- interpret the differing information about slice spacing and scanner specs in Atkinson et al. (2015)
- 185 to be typographic errors.
- The CT images of each skull were oriented in the frontal plane, beginning at the anterior part of
- the face (including the incisors) and progressing posteriorly to the occipital region and sagittal
- 188 crest, if present. As a result, any measurement along the anterior-posterior axis is mostly



189 influenced by the slice spacing, whereas width or height distances are less sensitive to this 190 parameter. Reading the DICOM files: Identification of the slice spacing problem 191 We used the 3D Slicer software (Fedorov et al., 2012) for scan processing. This is a free, open-192 193 source program for visualization, processing, segmentation, registration, and analysis of 3D 194 images and meshes. 195 196 Initially, all skull CT scans were expected to be imported into 3D Slicer following the same 197 sequence of steps with the DICOM Import module, regardless of specific slice spacing used 198 during the initial image acquisition process at WUSTL. This involves navigating to the directory 199 where the skull DICOM files are located; selecting the patient (individual), study, and series; and 200 clicking on "Load", resulting in the generation of a single volume that includes the entire skull, as 201 shown for skull W201 (Supplemental Information Figure 1). We were able to successfully follow 202 this process for most of the specimens: all skulls scanned with a 0.75 mm slice spacing (W001-203 W487) and most of those scanned with a 0.6 mm slice spacing (W670-W985). However, an 204 import warning with an error was generated for 182 of the scans with 0.6 mm slice spacing. 205 When scans for W488 to W669 were loaded into 3D Slicer, each skull generated ~50 volumes 206 instead of one. The number of volumes is different from one specimen to another, depending on 207 the size of the skull. For instance, 51 volumes were created for the specimen W584 208 (Supplemental Information Figure 2). When we visualized one of these 51 volumes (e.g., "2: *InnerEarSeq 0.6 U75u – acquisitionNumber 39*"), we realized that only part of the skull was 209 displayed, and this volume was comprised of 6 slices (Supplemental Information Figure 3). 210 211 In order to load the entire skull for these multivolume specimens, we navigated to the *Advanced* 212 option in the DICOM module and selected *Examine*. On that screen, we unchecked all 51 volumes of W584 and then re-checked only the last one, named in our example "2: InnerEarSeq 213 214 0.6 U75u" (Supplemental Information Figure 4). 215 After clicking on "Load" a warning message appeared indicating that "0.6 spacing was expected, 216 0.5 spacing was found between files [...]" (Supplemental Information Figure 5). Eventually, the 217 entire skull for W584 was loaded, but with a slice spacing of 0.58360656 mm, rather than the expected 0.60 mm (Supplemental Information Figure 6). The resultant spacing is different 218 219 depending on the skull, as this value is automatically calculated by 3D Slicer based on the 220 number of volumes per skull and slices within each volume. In these cases, within a volume there 221 is a constant spacing of 0.60 mm, but between volumes there is a spacing of 0.50 mm. In all 222 cases, the first two digits of the slice spacing are a constant (0.58) and spacing differences 223 become apparent in the thousandths position and beyond. The effect of the slice spacing mismatch on data collection 224 225 To demonstrate the effect of an erroneous slice spacing assignment of 0.58 mm instead of 0.60

mm on anatomical data collection and eventual measurement, we continue to use skull W584 as



- an example. As described above, we loaded the W584 DICOM files in 3D Slicer, which
- automatically assigned a slice spacing of 0.58360656 mm.
- Using a slice spacing of 0.58360656 mm the linear distance between a small fracture on the
- 230 incisal edge of the upper left central incisor and the posterior-most point of the skull in sagittal
- position (Supplemental Information Figure 7a) was estimated to be 173.3 mm. We then manually
- 232 changed the slice spacing to 0.60 mm to agree with the slice thickness indicated in the original
- 233 DICOM header file of this specimen (Supplemental Information Figure 7b). Using these data, we
- 234 collected the 3D coordinates of the same two landmarks and the linear distance between them
- was estimated to be 178.2 mm indicating a 4.9 mm difference between the same linear distance
- estimated on the image data that differed only in the assigned slice spacing (Supplemental
- 237 Information Figure 7c). In other words, the linear distance estimated on the 0.60 mm model for
- specimen W584 is 2.83% larger than that estimated from the 0.58 mm model. As quantitative
- 239 genetic analyses are highly sensitive to noise and the slice spacing discrepancy is inconsistently
- present across the pedigreed sample, we decided that this level of known error was unacceptable.
- To verify that the problem with slice spacing was in the DICOM files and not in the software 3D
- 242 Slicer, we loaded the CT scan of skull W584 into Amira-Avizo (Thermo Fisher Scientific,
- 243 Waltham, Massachusetts). Due to proprietary nature of this software, it was not possible to see
- 244 the slice spacing employed, but the same linear distance estimated between these two landmarks
- 245 was 173.73 mm, which is more similar to the distance obtained in 3D Slicer with the 0.58 mm
- slice spacing model (173.3 mm) than to the 0.60 mm model (178.2 mm). Given that both Amira-
- Avizo and 3D Slicer automatically load this skull scan with a 0.584 mm slice spacing, we
- 248 concluded that the problem is rooted in the DICOM files and not in the software. However, this
- 249 conclusion did not determine which slice spacing value is correct, thereby providing the most
- accurate reflection of the physical skull. Fortunately, the physical skulls are still available for
- study, which allowed us to solve this puzzle.

Comparison of linear measurement from virtual models and real skulls

- Next, we compared a highly replicable standard linear measurement from the CT scans and from
- 254 the original skeletal specimens. Two landmarks were selected to calculate this linear distance.
- 255 The first was prosthion (PR), defined as the most anterior point on the lingual surface of
- 256 maxillary I1 septum. The second landmark was basion (BA), defined as the midline point on the
- anterior margin of the foramen magnum (Figure 1).
- Although the PR-BA distance does not capture the maximum length of the skull, which is
- 259 typically calculated as the distance from PR to lambda (LD), BA was selected instead of LD due
- 260 to the methods employed during necropsy. The neurocranium of most of these skulls was
- sectioned to extract the brain, and in many cases, the posterior part of the foramen magnum was
- damaged, obliterating the opisthion (OP) landmark. Although the sectioned portion was
- reattached during the CT scan process to best approximate the amount of bone lost during
- sectioning, the reattachment process is a likely source of measurement error. Therefore, the PR-
- 265 BA distance is the most reliable measurement of cranial length.



- We created three sub-samples from the CT scans. We assigned individuals to Group 1, using the function sample() from the *base* package in R (R Core Team, 2018). Ten individuals were
- randomly selected from the scans that had a slice spacing of 0.75 mm and returned no warning
- 269 message related to slice spacing issues when imported with 3D Slicer (W001-W487).. The Group
- 270 1 specimen numbers were: W023, W031, W096, W188, W264, W281, W297, W343, W451 and
- W481. For Group 2, we used the same sample function to randomly select five individuals from
- 272 the CT scans that have a slice spacing of 0.60 mm and no slice spacing error message when
- loaded into 3D Slicer (W670-W985). The Group 2 specimen numbers were: W728, W781,
- W805, W914, and W955. Finally, for Group 3, we randomly selected five individuals between
- 275 W488 to W669, the specimens for whom a slice spacing error was returned when loading into 3D
- 276 Slicer, and for which we are unsure if the slice spacing is 0.60 mm (as per the DICOM file
- 277 heading) or 0.58 mm (automatically calculated by 3D Slicer and Amira-Avizo). The Group 3
- 278 specimen numbers were: W489, W535, W614, W620, and W650.
- 279 The PR-BA distance was iteratively measured 10 times for each specimen format, and therefore,
- 280 20 times for each individual in Group 1 (CT scan and physical skull) and 30 times for each
- individual in Groups 2 and 3. For individuals in Groups 2 and 3, the distance was measured 10
- 282 times from the CT scan with a 0.58 mm slice spacing, 10 more times from the CT scan with a
- 283 0.60 mm slice spacing, and 10 times from the physical skull. In Group 2, the manually introduced
- spacing is 0.58 mm, whereas it was 0.60 mm in Group 3. All CT data were collected by study
- author M.M.-M. All skull data were collected by coauthor K.L.K by using a caliper.
- Additionally, we compared our CT-derived measurements to the PR-BA distances calculated
- from landmark data collected by Joganic et al. (2018) from the physical skulls using a
- 288 microscribe MS digitizer (Revware Inc., Raleigh, North Carolina). The raw data with all the
- 289 measurements can be downloaded from the Supplemental Information (raw data.ods).
- 290 The study employed two statistical approaches to compare measurements. First, a pairwise
- Welch's t-test was applied to assess whether the medians of two independent samples (e.g.,
- 292 physical measurements vs. tomographic measurements) were statistically distinct. This test is
- 293 designed to evaluate differences in medians between two groups, accounting for potential
- 294 unequal variances. Second, we evaluated whether the single microscribe MS measurements
- reported by Joganic et al. (2018) fell within the 99% prediction interval for each sample group.
- 296 Both analyses were performed using R functions: the t_test() function from the *rstatix*
- 297 package (Kassambara, 2023), with var.equal = FALSE and paired = TRUE for the first
- approach, and the predict () function of the stats package (R Core Team, 2018) to estimate
- 299 prediction intervals for the second approach. The R script code that permits to create figures and
- run analyses can be downloaded from the Supplemental Information (r_script.R).

Results

- The comparison of the repeated PR-BA measurements for Group 1 are shown in Figure 2. For
- seven individuals the distribution of repeated measurements taken from CT scans with a slice
- 304 spacing of 0.75 mm overlap the interquartile range of the distribution of repeated measurements



- taken from the physical skulls. However, for one of the remaining three specimens (W096), the
- 306 CT-derived measurements overlap only with the smallest of the caliper-derived measurements.
- 307 Conversely, the CT-derived data for W451 were on average 1.5 mm larger than those
- measurements taken from the skull, and there is no overlap in the distribution of the two types of
- measurements. Finally, for W481, the largest CT measurement is almost identical to the smallest
- 310 measurement made on the skull, with the means of the two data sources differing by almost 1
- 311 mm. On average, within this group of 10 specimens, the mean of the CT-derived PR-BA distance
- 312 differs from that of the caliper-derived measurements by 0.18 mm. For six of the specimens, the
- 313 microscribe-derived measurements are larger than any of the repeated measurements taken from
- 314 the CT scans or the physical skulls. For three specimens, the measurements obtained from all
- 315 three sources overlap.. For the remaining specimen (W481), the microscribe measurement falls in
- 316 the upper range of values measured from the physical skull. All these differences represent less
- 317 than 1% of the average measurement.
- 318 The boxplots of the repeated measurements for each of the five specimens in Group 2 are shown
- 319 in Figure 3. For these specimens, the CT scan, physical skull, and microscribe data provided
- almost the exact same measurements for both W955 and W914. For W805, the CT and
- 321 microscribe measurements are almost identical, but the physical skull yielded a measurement that
- 322 is 1 mm smaller. For W728 and W781, the physical skull measurement is between 0.5 and 1 mm
- 323 smaller than that derived from the CT scan, and approximately 1.5 mm smaller than the
- 324 measurement calculated from the microscribe data. As a reminder, for this group, the automatic
- 325 slice spacing set by both software packages and the slice spacing indicated in the DICOM header
- are both 0.6 mm. When we manually re-set the slice spacing to 0.58 mm. PR-BA is 3-4 mm
- 327 smaller than the measurements taken using a slice spacing of 0.6 mm, with a microscribe, or from
- 328 the physical skull. Thus, 0.6 mm is the appropriate slice spacing for individuals W670–W985.
- 329 The results for Group 3 are presented in Figure 4. For these specimens, we see the reverse of
- 330 what was observed for Group 2. Here, the measurements from the CT scans with slice spacing
- manually set to 0.6 mm were more than 3 to 5 mm greater than the values obtained from the CT
- scans with 0.58 slice spacing automatically set, the physical skulls, and the microscribe.
- The results of the pairwise Welch's t-test between all the samples in the three groups are shown in
- Table 1. In Group 1, the comparison of PR-BA distances between the original measurements and
- 335 the CT-0.75 mm ones were not statistically different (p > 0.05), with the exception of W451 (p <
- 336 0.0001). In Group 3, comparisons between the original measurements and the CT-0.58 mm scans
- across all skulls revealed no statistically significant differences (p > 0.05). In contrast,
- comparisons between the original measurements and the CT-0.60 mm scans, as well as between
- the CT-0.58 mm and CT-0.60 mm scans, showed highly statistically significant differences
- (p < 0.0001). In Group 2, the situation is the opposite as in Group 3. When distances between CT-
- 341 0.60 mm and the original measurements are compared, they are not statistically different (p >
- 0.05), with the exception of skull W805 (p < 0.0001). The remaining pairwise comparisons were
- 343 significantly different (p < 0.0001).
- The microscribe-derived measurements taken by Joganic et al. (2018) from the physical skulls
- offer an opportunity to further test the fit between caliper-derived measurements and the various



- 346 CT model-derived measurements. We analyzed these microscribe measurements to see if they
- 347 correspond with the prediction intervals of the other measurement techniques (confidence = 0.99)
- for any of the four sample groups (original, CT_0.75 mm, CT_0.60 mm, and CT_0.58 mm)
- 349 (Tables 2 and 3). Based on statistical tests shown in Table 1, we expect that:
- 350 The microscribe-derived measurements are within the prediction limits in all the caliper-derived
- 351 *measurements taken from the physical skulls in Groups 1, 2 and 3.* We found that the microscribe-
- derived measurements are within the prediction interval of the caliper-derived measurement for
- 353 17 out of 20 skulls (85%, Tables 2 and 3). The exceptions are W451 (Group 1, Table 2) and
- W728 and W805 (both in Group 2, Table 3). For these three individuals, the microscribe-derived
- 355 measurements are within less than 1 mm of the upper limits of the caliper-derived measurements
- 356 (0.86 mm, 0.17 mm and 0.18 mm, respectively). In terms of anatomical variation, this represents
- less than 1% of the overall measurement. Therefore, even though the difference is statistically
- 358 significant, the distinction between the microscribe- and caliper-derived does not represent a
- 359 significant amount of measurement error from an anatomical sciences perspective.
- The microscribe-derived measurements are within the range of values calculated from the
- 361 *CT*_0.75 mm models of skulls from Group 1 (i.e., the correct slice spacing). We found that the
- 362 microscribe-derived measurements are within the limits of the CT_0.75 mm sample for 8 out of
- 363 10 individuals, with the exception of W096 and W343 (Table 2). For these two individuals, the
- 364 microscribe-derived values are 1.19 mm and 0.43 mm above the upper limits of the CT_0.75 mm
- 365 model-derived values, respectively. As noted in the previous paragraph, although statistically
- significant, this does not represent measurement error greater than 1%.
- 367 The microscribe-derived measurements are within the range of values calculated from the
- 368 *CT*_0.60 mm models of skulls from *Group 2* (i.e., the correct slice spacing). As expected, for 4 out
- 369 5 skulls, the microscribe-derived measurement is within the range of values obtained from the
- 370 CT 0.60 mm model (Table 3). The one exception is W781, for which the microscribe-derived
- 371 value is 0.11 mm above the upper end of the CT_0.60 mm model-derived values (less than 1%
- 372 measurement error).
- 373 The microscribe-derived measurements are within the range of values calculated from the
- 374 *CT*_0.58 mm in Group 3 (i.e., the correct slice spacing). For 4 of 5 individuals, the microscribe-
- derived measurement is within the range of values from the CT scan models set to a slice spacing
- of 0.58 mm (Table 3). The one exception is W620, whose microscribe measurement is also 0.11
- 377 mm above the upper limit (less than 1% measurement error).
- 378 The microscibe-derived measurements are below the measurements derived from the CT-0.60 mm
- 379 model for individuals in Group 3 (as the slice spacing should be 0.58 mm). For all five
- individuals, the microscribe measurements are 1.97 mm to 2.76 mm below the range of values
- obtained from the CT_0.60 mm models (Table 3).
- 382 The microscribe-derived measurements are above the measurements derived from the CT-0.58
- 383 *mm model for individuals in Group 2*. As expected, all five skulls are 2.86 mm to 3.75 mm above
- the prediction upper limits of CT_0.58 mm samples (Table 3).



- Overall, our results indicate that in 43 out of 50 comparisons (86%), the microscribe-derived data
- 386 fit either within or very close to the ranges of both the caliper-derived measurements and those
- taken from the CT models with the correct slice spacing. As the microscribe data are either
- 388 significantly larger or smaller than the measurements taken from the CT models with incorrect
- 389 slice spacing, our designations of the correct identity of the slice spacing values for the three
- 390 groups are supported.
- 391 In conclusion, our results show that the automatically calculated slice spacings in 3D Slicer
- 392 faithfully represents the physical skulls (0.75 mm for Group 1, 0.60 mm for Group 2, and 0.58
- 393 mm for Group 3).

Discussion

- 395 Here, we described the investigation of a mismatch between manually reported and automatically
- detected slice spacing for a subset of CT scans acquired for 985 SNPRC baboon skulls. We
- 397 walked through our process for identifying the source of the mismatch (the metadata reported
- 398 with the associated DICOM files on the data aggregation site), and our process for determining
- 399 which CT slice spacing value is the best match for the physical skull, using both caliper- and
- 400 microscribe-derived measurements for reference. We found that the automatic detection of slice
- 401 spacing in both 3D Slicer and Amira-Avizo creates a 3D model that best reflects the physical
- skull, although this value is hidden in the proprietary Amira-Avizo and made obvious in 3D
- 403 Slicer.
- The use of virtual paleontology is significantly increasing (Cunningham et al., 2014). Although
- 405 there are some studies comparing physical and virtual measurements (Tolentino et al., 2018),
- 406 different virtual models of the same fossils (Díez Díaz et al., 2021), or the comparison of
- 407 different parameters of the same virtual model to find the optimal combination (Pérez-Ramos &
- 408 Figueirido, 2020), most scientists with access to the virtual models do not have access to the
- original specimen. Therefore, DICOM files, surface meshes, or other 3D data must be assumed to
- 410 be a faithful representation of the original and this assumption cannot easily be tested.
- 411 The great benefits of these virtual models are undeniable. For example, scans can help to limit the
- 412 handling of valuable and irreplaceable specimens (Gilissen, 2009). They also make access to
- 413 specimens more equitable to those with access to the internet and adequate digital storage.
- However, scientists must be mindful that they are dealing with a digital model of the original
- 415 specimen that is the result of many procedural steps (Noumeir & Pambrun, 2012; Li et al., 2016).
- Each parameter value that drives the creation of the virtual model has the potential to contribute
- 417 to the creation of an unrealistic or unfaithful model, compromising its scientific value.
- 418 We were unable to contact the technicians that scanned the SNPRC baboon CT scans of
- 419 specimens W488 to W669, so we suspect that in the process of scanning or of converting the raw
- 420 file into DICOM files, some parameters may have been unintentionally modified, leading to the
- 421 slice spacing issues. 3D Slicer brought this issue to our attention with a warning message.
- 422 Although Amira-Avizo automatically detected the most appropriate slice spacing, this adjustment



- was invisible to the user, which could lead to unforeseen complications for investigators less
- 424 familiar with scanning protocols.
- 425 It is critical that such analytical decisions made by any software are made transparent and any
- 426 issues encountered during data import are communicated clearlyi. For instance, while Amira-
- 427 Avizo appeared to handle the data without errors and loaded the data with a seemingly correct
- 428 spacing value, it did so without notifying the user of any assumptions or modifications. In
- 429 contrast, 3D Slicer identified a spacing inconsistency and halted the import process until the user
- explicitly confirmed how to proceed. Moreover, 3D Slicer clearly documented the adjustments it
- 431 applied (i.e., regularizing slice spacing), thereby allowing the user to verify the changes. While
- automatic corrections can be helpful, undetected or incorrect assumptions—such as those
- 433 potentially made by Amira-Avizo—pose a risk to data integrity. As done by 3D Slicer, any
- inconsistency in the data should be communicated to the user to ensure transparency and
- 435 reproducibility.
- 436 In addition to determining the proper slice spacing value, our study also raises two other
- 437 interesting points relevant to the use of 3D models in anatomical research. First, as is
- 438 immediately evident in Figures 2 and 3, every method of measurement collection includes error.
- 439 Sometimes these different measurement collection approaches return almost identical values, but
- 440 this was only the case for 6 of the 20 specimens (30%) included in our study. For the most part,
- 441 microscribe data tend to return relative increases in the measurement value, whereas CT-derived
- 442 measurements and caliper-derived measurements do not consistently yield relatively larger or
- smaller values compared to each other. Just over 50% of the individuals in our study reported
- smaller caliper-derived distances compared to the CT-derived distance. When looking at these
- results, we only measured one cranial dimension, so the box plots are reporting the variation in
- 446 repeated measurements. This observation echoes caution, as has been voiced previously, in both
- 447 industry and medical cases (Lascala, Panella & Margues, 2004; Lund, Gröndahl & Gröndahl,
- 2009; Carmignato, 2012). While these discrepancies could be worrisome, the reality is that the
- 449 measurement differences are well below the level of measurement error that most anatomists
- 450 consider acceptable (<3%) (Stull et al., 2014).
- 451 A second observation that is relevant to our results pertains to the confidence with which we
- imbue CT scan data. Ford and Decker (2016) ran a study of 20 human crania CT scanned with
- 453 different slice thicknesses, finding that placing landmarks on models created with 2 mm or
- 454 greater slice spacing returns questionable results. Fortunately, the SNPRC baboon skulls were all
- scanned well below this threshold, with slice spacing of 0.58 mm, 0.6 mm, or 0.75 mm. The key,
- as we discovered, lies in accurately determining which slice spacing value corresponds to each
- 457 specimen. From our investigation, we conclude that:
- Individuals W001 to W487 were scanned with a slice spacing of 0.75 mm.
- Individuals W488 to W669 were scanned with a slice spacing of 0.58 mm.
- Individuals W670 to W985 were scanned with a slice spacing of 0.60 mm.



461 It cannot be overstated that the simplicity of this discovery greatly masks the amount of time required to resolve it. More than 250-person hours of effort, spread over 8 months were dedicated 462 to resolving this issue. First, we had to trouble-shoot the import error, ultimately realizing that the 463 464 slice spacing parameter was the cause. We then had to identify which specimens returned the 465 import error, and therefore had a slice spacing mismatch. This turned into an investigation to 466 ascertain which slice spacing value was correct. This effort ultimately reduced a 3–5% 467 measurement bias in nearly 20% of the sample, primarily affecting measurements along the 468 anterior-posterior axis.

Conclusions

- 470 While digital data aggregators such as MorphoSource provide invaluable access to morphological
- datasets, some level of quality control should be implemented to ensure the reliability of the
- shared data. Additionally, direct access to physical specimens remains essential; many analytical
- 473 procedures and validations—such as those conducted in this study—would not have been
- 474 possible without firsthand examination of the physical skulls.
- Resolving this puzzle cost our research group hundreds of hours of researcher time. However, we
- are now aware of a source of measurement error that could have undermined our genetic
- analyses. We have also identified the correct slice spacing parameter values that can be shared
- 478 with MorphoSource, so that these scans can be included in semi-automated data collection
- 479 protocols.
- We share this cautionary tale to strongly encourage investigators to take the time to ensure that
- 481 they are familiar with the nuances of the scans from which they are collecting data (as we
- 482 imagine the temptation to overlook the loading error would be strong). Additionally, we hope that
- 483 our experience can be cited as justification to funding agencies when asking for the financial
- support needed to carefully process digital images to avoid errors, both on the data-collection side
- as well as the resource-sharing side of the process.

_ .

Funding statement

- 488 This research was funded by the European Research Council within the European Union's
- 489 Horizon Europe (ERC-2021-ADG, Tied2Teeth, project number 101054659).
- 490 Research at the CENIEH is supported by funding from the Ministerio de Ciencia e Innovación
- 491 Project PID2021-122355NB-C33 financed by MCIN/ AEI/10.13039/501100011033/ FEDER,
- 492 UE.

486

- 493 This investigation used resources that were supported by the Southwest National Primate
- 494 Research Center grant P51 OD011133 from the Office of Research Infrastructure Programs,
- National Institutes of Health, and also by the National Science Foundation grant 2007-10
- 496 (Developmental Genetic basis of primate craniofacial variation, and human origins BCS-
- 497 0725227).



498 There was no additional external funding received for this study.

Acknowledgements

- We thank the European Union, the European Research Council, and the funding agencies for their
- support. The views and opinions expressed in this article are those of the author(s) alone and do
- not necessarily reflect the official policy or position of the United States government or any of its
- agencies, the European Union, or the European Research Council. Neither the European Union
- nor the granting authority can be held responsible for them. The information presented is based
- on the author(s)' research and analysis and is intended for educational and informational purposes
- only, with the author(s) assuming full responsibility for the content and any conclusions drawn

507 **References**

- Atkinson EG, Rogers J, Mahaney MC, Cox LA, Cheverud JM. 2015. Cortical Folding of the Primate Brain: An Interdisciplinary Examination of the Genetic Architecture, Modularity, and Evolvability of a Significant Neurological Trait in Pedigreed Baboons (Genus Papio). *Genetics* 200:651–665. DOI: 10.1534/genetics.114.173443.
- Bannister JJ, Crites SR, Aponte JD, Katz DC, Wilms M, Klein OD, Bernier FPJ, Spritz RA, Hallgrímsson B, Forkert ND. 2020. Fully Automatic Landmarking of Syndromic 3D Facial Surface Scans Using 2D Images. *Sensors* 20:3171. DOI: 10.3390/s20113171.
- Barger N, Martín JS, Boyle EK, Richmond M, Diogo R. 2021. The Visible Ape Project: A free, comprehensive, web-based anatomical atlas for scientists and veterinarians designed to raise public awareness about apes. *Evolutionary Anthropology: Issues, News, and Reviews* 30:160–170. DOI: 10.1002/evan.21896.
- Bastir M, García-Martínez D, Williams SA, Recheis W, Torres-Sánchez I, García Río F, Oishi M, Ogihara N. 2017. 3D geometric morphometrics of thorax variation and allometry in Hominoidea. *Journal of Human Evolution* 113:10–23. DOI: 10.1016/j.jhevol.2017.08.002.
- Blackburn DC, Boyer DM, Gray JA, Winchester J, Bates JM, Baumgart SL, Braker E, Coldren D, Conway KW, Rabosky AD, de la Sancha N, Dillman CB, Dunnum JL, Early CM, Frable BW, Gage MW, Hanken J, Maisano JA, Marks BD, Maslenikov KP, McCormack JE, Nagesan RS, Pandelis GG, Prestridge HL, Rabosky DL, Randall ZS, Robbins MB, Scheinberg LA, Spencer CL, Summers AP, Tapanila L, Thompson CW, Tornabene L, Watkins-Colwell GJ, Welton LJ, the oVert Project Team, Stanley EL. 2024. Increasing the impact of vertebrate scientific collections through 3D imaging: The openVertebrate (oVert) Thematic Collections Network. *BioScience* 74:169–186. DOI: 10.1093/biosci/biad120.
- Boissinot S, Alvarez L, Giraldo-Ramirez J, Tollis M. 2014. Neutral nuclear variation in Baboons (genus apio) provides insights into their evolutionary and demographic histories. *American Journal of Physical Anthropology* 155:621–634. DOI: 10.1002/ajpa.22618.
- Boklage ChE. 1987. Developmental differences between singletons and twins in distributions of dental diameter asymmetries. *American Journal of Physical Anthropology* 74:319–331.
- Boukamcha H, Hallek M, Smach F, Atri M. 2017. Automatic landmark detection and 3D Face data extraction. *Journal of Computational Science* 21:340–348. DOI: 10.1016/j.jocs.2016.11.015.



- Boyer DM, Gunnell GF, Kaufman S, McGeary TM. 2016. MORPHOSOURCE: ARCHIVING AND SHARING 3-D DIGITAL SPECIMEN DATA. *The Paleontological Society Papers* 22:157–181. DOI: 10.1017/scs.2017.13.
- Bradtmöller M, Pastoors A, Slizewski A, Weniger G-C. 2010. NESPOS A Digital Archive and Platform for Pleistocene Archaeology. In: Curdt C, Bareth G eds. *Proceedings of the Data Management Workshop*. 13–17.
- Bruner E. 2004. Geometric morphometrics and paleoneurology: brain shape evolution in the genus Homo. *Journal of Human Evolution* 47:279–303. DOI: doi: DOI: 10.1016/j.jhevol.2004.03.009.
- Buser TJ, Boyd OF, Cortés Á, Donatelli CM, Kolmann MA, Luparell JL, Pfeiffenberger JA, Sidlauskas BL, Summers AP. 2020. The Natural Historian's Guide to the CT Galaxy: Step-by-Step Instructions for Preparing and Analyzing Computed Tomographic (CT) Data Using Cross-Platform, Open Access Software. *Integrative Organismal Biology* 2:obaa009. DOI: 10.1093/iob/obaa009.
- Carmignato S. 2012. Accuracy of industrial computed tomography measurements: Experimental results from an international comparison. *CIRP Annals* 61:491–494. DOI: 10.1016/j.cirp.2012.03.021.
- Clark K, Vendt B, Smith K, Freymann J, Kirby J, Koppel P, Moore S, Phillips S, Maffitt D, Pringle M, Tarbox L, Prior F. 2013. The Cancer Imaging Archive (TCIA): Maintaining and Operating a Public Information Repository. *Journal of Digital Imaging* 26:1045—1057. DOI: 10.1007/s10278-013-9622-7.
- Conde-Valverde M, Martínez I, Quam RM, Bonmatí A, Lorenzo C, Velez AD, Martínez-Calvo C, Arsuaga JL. 2019. The cochlea of the Sima de los Huesos hominins (Sierra de Atapuerca, Spain): New insights into cochlear evolution in the genus *Homo. Journal of Human Evolution* 136:102641. DOI: 10.1016/j.jhevol.2019.102641.
- Copes LE, Lucas LM, Thostenson JO, Hoekstra HE, Boyer DM. 2016. A collection of non-human primate computed tomography scans housed in MorphoSource, a repository for 3D data. *Scientific Data* 3:160001. DOI: 10.1038/sdata.2016.1.
- Cox LA, Mahaney MC, VandeBerg JL, Rogers J. 2006. A second-generation genetic linkage map of the baboon (*Papio hamadryas*) genome. *Genomics* 88:274–281. DOI: 10.1016/j.ygeno.2006.03.020.
- Cunningham JA, Rahman IA, Lautenschlager S, Rayfield EJ, Donoghue PCJ. 2014. A virtual world of paleontology. *Trends in Ecology & Evolution* 29:347–357. DOI: 10.1016/j.tree.2014.04.004.
- Davies TG, Rahman IA, Lautenschlager S, Cunningham JA, Asher RJ, Barrett PM, Bates KT, Bengtson S, Benson RBJ, Boyer DM, Braga J, Bright JA, Claessens LPAM, Cox PG, Dong X-P, Evans AR, Falkingham PL, Friedman M, Garwood RJ, Goswami A, Hutchinson JR, Jeffery NS, Johanson Z, Lebrun R, Martínez-Pérez C, Marugán-Lobón J, O'Higgins PM, Metscher B, Orliac M, Rowe TB, Rücklin M, Sánchez-Villagra MR, Shubin NH, Smith SY, Starck JM, Stringer C, Summers AP, Sutton MD, Walsh SA, Weisbecker V, Witmer LM, Wroe S, Yin Z, Rayfield EJ, Donoghue PCJ. 2017. Open data and digital morphology. *Proceedings of the Royal Society B: Biological Sciences* 284:20170194. DOI: 10.1098/rspb.2017.0194.
- Diamond KM, Burtner AE, Siddiqui D, Alvarado K, Leake S, Rolfe S, Zhang C, Kwon RY, Maga AM. 2023. Examining craniofacial variation among crispant and mutant zebrafish models of human skeletal diseases. *Journal of Anatomy* 243:66–77. DOI: 10.1111/joa.13847.
- Díez Díaz V, Mallison H, Asbach P, Schwarz D, Blanco A. 2021. Comparing surface digitization techniques in palaeontology using visual perceptual metrics and distance computations between 3D meshes. *Palaeontology* 64:179–202. DOI: 10.1111/pala.12518.



- Edgar H, Daneshvari Berry S, Moes E, Adolphi N, Bridges P, Nolte K. 2020. *New Mexico Decedent Image Database. Office of the Medical Investigator*. University of New Mexico.
- Fedorov A, Beichel R, Kalpathy-Cramer J, Finet J, Fillion-Robin J-C, Pujol S, Bauer C, Jennings D, Fennessy F, Sonka M, Buatti J, Aylward S, Miller JV, Pieper S, Kikinis R. 2012. 3D Slicer as an image computing platform for the Quantitative Imaging Network. *Magnetic Resonance Imaging* 30:1323–1341. DOI: 10.1016/j.mri.2012.05.001.
- Ford JM, Decker SJ. 2016. Computed tomography slice thickness and its effects on three-dimensional reconstruction of anatomical structures. *Journal of Forensic Radiology and Imaging* 4:43–46. DOI: 10.1016/j.jofri.2015.10.004.
- García-Campos C, Martinón-Torres M, Martín-Francés L, Modesto-Mata M, Martínez de Pinillos M, Arsuaga JL, Bermúdez de Castro JM. 2019. Enamel and dentine dimensions of the Pleistocene hominins from Atapuerca (Burgos, Spain): A comparative study of canine teeth. *Comptes Rendus Palevol* 18:72–89. DOI: 10.1016/j.crpv.2018.06.004.
- Garn SM, Lewis AB, Kerewsky RS. 1966. Sexual Dimorphism in the Bucolingual Tooth Diameter. *Journal of Dental Research* 45:1819.
- Garrod DAE, Buxton LHD, Smith GE, Bate DMA, Spiller RC, Hinton MAC, Fischer P. 1928. Excavation of a Mousterian Rock-Shelter at Devil's Tower, Gibraltar. *The Journal of the Royal Anthropological Institute of Great Britain and Ireland* 58:33–113.
- Gilissen E. 2009. Museum collections, scanning, and data access. *Journal of Anthropological Sciences* 87:223–226.
- Hansman CF. 1966. Growth of Interorbital Distance and Skull Thickness as Observed in Roentgenographic Measurements. *Radiology* 86:87–96. DOI: 10.1148/86.1.87.
- Havill LM, Allen MR, Bredbenner TL, Burr DB, Nicolella DP, Turner CH, Warren DM, Mahaney MC. 2010. Heritability of lumbar trabecular bone mechanical properties in baboons. *Bone* 46:835–840. DOI: 10.1016/j.bone.2009.11.002.
- Hlusko LJ, Schmitt CA, Monson TA, Brasil MF, Mahaney MC. 2016. The integration of quantitative genetics, paleontology, and neontology reveals genetic underpinnings of primate dental evolution. *Proceedings of the National Academy of Sciences* 113:9262–9267. DOI: 10.1073/pnas.1605901113.
- Hlusko LJ, Suwa G, Kono RT, Mahaney MC. 2004. Genetics and the evolution of primate enamel thickness: A baboon model. *American Journal of Physical Anthropology* 124:223–233. DOI: 10.1002/ajpa.10353.
- Hlusko LJ, Weiss KM, Mahaney MC. 2002. Statistical genetic comparison of two techniques for assessing molar crown size in pedigreed baboons. *American Journal of Physical Anthropology* 117:182–189. DOI: 10.1002/ajpa.10022.
- Jacobsen A, de Miranda Azevedo R, Juty N, Batista D, Coles S, Cornet R, Courtot M, Crosas M, Dumontier M, Evelo CT, Goble C, Guizzardi G, Hansen KK, Hasnain A, Hettne K, Heringa J, Hooft RWW, Imming M, Jeffery KG, Kaliyaperumal R, Kersloot MG, Kirkpatrick CR, Kuhn T, Labastida I, Magagna B, McQuilton P, Meyers N, Montesanti A, van Reisen M, Rocca-Serra P, Pergl R, Sansone S-A, da Silva Santos LOB, Schneider J, Strawn G, Thompson M, Waagmeester A, Weigel T, Wilkinson MD, Willighagen EL, Wittenburg P, Roos M, Mons B, Schultes E. 2020. FAIR Principles: Interpretations and Implementation Considerations. *Data Intelligence* 2:10–29. DOI: 10.1162/dint_r_00024.
- Joganic JL, Heuzé Y. 2019. Allometry and advancing age significantly structure craniofacial variation in adult female baboons. *Journal of Anatomy* 235:217–232. DOI: 10.1111/joa.13005.
- Joganic JL, Willmore KE, Richtsmeier JT, Weiss KM, Mahaney MC, Rogers J, Cheverud JM. 2018. Additive genetic variation in the craniofacial skeleton of baboons (genus Papio) and



- its relationship to body and cranial size. *American Journal of Physical Anthropology* 165:269–285. DOI: 10.1002/ajpa.23349.
- Johnson Z, Brent L, Alvarenga JC, Comuzzie AG, Shelledy W, Ramirez S, Cox L, Mahaney MC, Huang Y-Y, Mann JJ, Kaplan JR, Rogers J. 2015. Genetic Influences on Response to Novel Objects and Dimensions of Personality in Papio Baboons. *Behavior Genetics* 45:215–227. DOI: 10.1007/s10519-014-9702-6.
- Jolly C. 2003. Cranial anatomy and baboon diversity. *The Anatomical Record Part A:* Discoveries in Molecular, Cellular, and Evolutionary Biology 275A:1043–1047. DOI: 10.1002/ar.a.10121.
- Kang SH, Jeon K, Kang S-H, Lee S-H. 2021. 3D cephalometric landmark detection by multiple stage deep reinforcement learning. *Scientific Reports* 11:17509. DOI: 10.1038/s41598-021-97116-7.
- Kassambara A. 2023. rstatix: Pipe-Friendly Framework for Basic Statistical Tests.
- Kos MZ, Carless MA, Blondell L, Leland MM, Knape KD, Göring HHH, Szabó CÁ. 2021. Whole Genome Sequence Data From Captive Baboons Implicate RBFOX1 in Epileptic Seizure Risk. *Frontiers in Genetics* 12. DOI: 10.3389/fgene.2021.714282.
- Lascala C, Panella J, Marques M. 2004. Analysis of the accuracy of linear measurements obtained by cone beam computed tomography (CBCT-NewTom). *Dentomaxillofacial Radiology* 33:291–294. DOI: 10.1259/dmfr/25500850.
- Lázaro GR, Neubauer S, Gunz P, Bruner E. 2020. Ontogenetic changes of diploic channels in modern humans. *American Journal of Physical Anthropology* 173:96–111. DOI: 10.1002/ajpa.24085.
- Lebre R, Silva LB, Costa C. 2020. A Cloud-Ready Architecture for Shared Medical Imaging Repository. *Journal of Digital Imaging* 33:1487–1498. DOI: 10.1007/s10278-020-00373-7.
- Lebrun R, Orliac MJ. 2016. MORPHOMUSEUM: AN ONLINE PLATFORM FOR PUBLICATION AND STORAGE OF VIRTUAL SPECIMENS. *The Paleontological Society Papers* 22:183–195. DOI: 10.1017/scs.2017.14.
- Li X, Morgan PS, Ashburner J, Smith J, Rorden C. 2016. The first step for neuroimaging data analysis: DICOM to NIfTI conversion. *Journal of Neuroscience Methods* 264:47–56. DOI: 10.1016/j.jneumeth.2016.03.001.
- Lund H, Gröndahl K, Gröndahl H-G. 2009. Accuracy and precision of linear measurements in cone beam computed tomography Accuitomo® tomograms obtained with different reconstruction techniques. *Dentomaxillofacial Radiology* 38:379–386. DOI: 10.1259/dmfr/15022357.
- Mahaney MC, Karere GM, Rainwater DL, Voruganti VS, Dick Jr EJ, Owston MA, Rice KS, Cox LA, Comuzzie AG, VandeBerg JL. 2018. Diet-induced early-stage atherosclerosis in baboons: Lipoproteins, atherogenesis, and arterial compliance. *Journal of Medical Primatology* 47:3–17. DOI: 10.1111/jmp.12283.
- Maples WR, McKern TW. 1967. A preliminary report on classification of the Kenya baboon. In: Vartborg H ed. *The baboon in medical research*. Austin, TX: University of Texas Press, 13–22.
- Martin LJ, Mahaney MC, Bronikowski AM, Dee Carey K, Dyke B, Comuzzie AG. 2002. Lifespan in captive baboons is heritable. *Mechanisms of Ageing and Development* 123:1461–1467. DOI: 10.1016/S0047-6374(02)00083-0.
- Martínez de Pinillos M, Martinón-Torres M, Martín-Francés L, Arsuaga JL, Bermúdez de Castro JM. 2017. Comparative analysis of the trigonid crests patterns in Homo antecessor molars at the enamel and dentine surfaces. *Quaternary International* 433:189–198. DOI: 10.1016/j.quaint.2015.08.050.



- Martín-Francés L, Martinón-Torres M, Pinillos MM de, García-Campos C, Zanolli C, Bayle P, Modesto-Mata M, Arsuaga JL, Castro JMB de. 2020. Crown tissue proportions and enamel thickness distribution in the Middle Pleistocene hominin molars from Sima de los Huesos (SH) population (Atapuerca, Spain). *PLOS ONE* 15:e0233281. DOI: 10.1371/journal.pone.0233281.
- Nelson G. 2014. IDigBio: The US National Science Foundation's National Resource for Digitization of Biological and Palobiological Collections. In: *Geological Society of America*, *Annual Meeting*. Vancouver (Canada),.
- Nelson G, Paul DL. 2019. DiSSCo, iDigBio and the Future of Global Collaboration. *Biodiversity Information Science and Standards*. DOI: 10.3897/biss.3.37896.
- Nguyen V, Alves Pereira LF, Liang Z, Mielke F, Van Houtte J, Sijbers J, De Beenhouwer J. 2022. Automatic landmark detection and mapping for 2D/3D registration with BoneNet. *Frontiers in Veterinary Science* 9. DOI: 10.3389/fvets.2022.923449.
- Noumeir R, Pambrun J-F. 2012. Teaching DICOM by Problem Solving. *Journal of Digital Imaging* 25:653–661. DOI: 10.1007/s10278-012-9471-9.
- Palancar CA, García Martínez D, Cáceres Monllor DA, Perea Pérez B, Ferreira MT, Bastir M. 2021. Geometric morphometrics of the human cervical vertebrae: sexual and population variations.
- Pérez-Ramos A, Figueirido B. 2020. Toward an "Ancient" Virtual World: Improvement Methods on X-ray CT Data Processing and Virtual Reconstruction of Fossil Skulls. *Frontiers in Earth Science* 8. DOI: 10.3389/feart.2020.00345.
- Pickering SP. 1930. Correlation of brain and head measurements, and relation of brain shape and size to shape and size of the head. *American Journal of Physical Anthropology* 15:1–52. DOI: 10.1002/ajpa.1330150102.
- R Core Team. 2018. *R: A Language and Environment for Statistical Computing*. Vienna, Austria: R Foundation for Statistical Computing.
- Robinson JA, Belsare S, Birnbaum S, Newman DE, Chan J, Glenn JP, Ferguson B, Cox LA, Wall JD. 2019. Analysis of 100 high-coverage genomes from a pedigreed captive baboon colony. *Genome Research* 29:848–856. DOI: 10.1101/gr.247122.118.
- Robinson C, Terhune CE. 2017. Error in geometric morphometric data collection: Combining data from multiple sources. *American Journal of Physical Anthropology* 164:62–75. DOI: 10.1002/ajpa.23257.
- Rogers J, Mahaney MC, Witte SM, Nair S, Newman D, Wedel S, Rodriguez LA, Rice KS, Slifer SH, Perelygin A, Slifer M, Palladino-Negro P, Newman T, Chambers K, Joslyn G, Parry P, Morin PA. 2000. A Genetic Linkage Map of the Baboon (*Papio hamadryas*) Genome Based on Human Microsatellite Polymorphisms. *Genomics* 67:237–247. DOI: 10.1006/geno.2000.6245.
- Rolfe S, Pieper S, Porto A, Diamond K, Winchester J, Shan S, Kirveslahti H, Boyer D, Summers A, Maga AM. 2021. SlicerMorph: An open and extensible platform to retrieve, visualize and analyse 3D morphology. *Methods in Ecology and Evolution* 12:1816–1825. DOI: 10.1111/2041-210X.13669.
- Roseman CC, Willmore KE, Rogers J, Hildebolt C, Sadler BE, Richtsmeier JT, Cheverud JM. 2010. Genetic and environmental contributions to variation in baboon cranial morphology. *American Journal of Physical Anthropology* 143:1–12. DOI: 10.1002/ajpa.21341.
- Schug GR, Killgrove K, Atkin A, Baron K. 2020. 3D Dead: Ethical Considerations in Digital Human Osteology. *Bioarchaeology International* 4:217–230. DOI: 10.5744/bi.2020.3008.



- Shearer BM, Cooke SB, Halenar LB, Reber SL, Plummer JE, Delson E, Tallman M. 2017. Evaluating causes of error in landmark-based data collection using scanners. *PLOS ONE* 12:e0187452. DOI: 10.1371/journal.pone.0187452.
- Sherwood RJ, Duren DL, Havill LM, Rogers J, Cox LA, Towne B, Mahaney MC. 2008. A Genomewide Linkage Scan for Quantitative Trait Loci Influencing the Craniofacial Complex in Baboons (Papio hamadryas spp.). *Genetics* 180:619–628. DOI: 10.1534/genetics.108.090407.
- Shi JJ, Westeen EP, Rabosky DL. 2018. Digitizing extant bat diversity: An open-access repository of 3D μ CT-scanned skulls for research and education. *PLOS ONE* 13:e0203022. DOI: 10.1371/journal.pone.0203022.
- Singer RA, Love KJ, Page LM. 2018. A survey of digitized data from U.S. fish collections in the iDigBio data aggregator. *PLOS ONE* 13:e0207636. DOI: 10.1371/journal.pone.0207636.
- Spake L, Nicholas G, Cardoso HFV. 2020. The digital lives of Ancestors: Ethical and intellectual property considerations surrounding the 3-D recording of human remains. In: *Working with and for Ancestors*. Routledge,.
- Spradling KD, Glenn JP, Garcia R, Shade RE, Cox LA. 2013. The Baboon Kidney Transcriptome: Analysis of Transcript Sequence, Splice Variants, and Abundance. *PLOS ONE* 8:e57563. DOI: 10.1371/journal.pone.0057563.
- Stull KE, Tise ML, Ali Z, Fowler DR. 2014. Accuracy and reliability of measurements obtained from computed tomography 3D volume rendered images. *Forensic Science International* 238:133–140. DOI: 10.1016/j.forsciint.2014.03.005.
- Sutton MD. 2008. Tomographic techniques for the study of exceptionally preserved fossils. *Proceedings of the Royal Society B: Biological Sciences* 275:1587–1593. DOI: 10.1098/rspb.2008.0263.
- Szabó CÁ, Salinas FS. 2021. The baboon in epilepsy research: Revelations and challenges. *Epilepsy & Behavior* 121:108012. DOI: 10.1016/j.yebeh.2021.108012.
- Tolentino E de S, Yamashita FC, de Albuquerque S, Walewski LA, Iwaki LCV, Takeshita WM, Silva MC. 2018. Reliability and accuracy of linear measurements in cone-beam computed tomography using different software programs and voxel sizes. *Journal of Conservative Dentistry and Endodontics* 21:607. DOI: 10.4103/JCD.JCD_314_18.
- Tsukayama P, Boolchandani M, Patel S, Pehrsson EC, Gibson MK, Chiou KL, Jolly CJ, Rogers J, Phillips-Conroy JE, Dantas G. 2018. Characterization of Wild and Captive Baboon Gut Microbiota and Their Antibiotic Resistomes. *mSystems* 3:10.1128/msystems.00016-18. DOI: 10.1128/msystems.00016-18.
- Uetz PH, Patel M, Gbadamosi Z, Nguyen A, Shoope S. 2024. A Reference Database of Reptile Images. *Taxonomy* 4:723–732. DOI: 10.3390/taxonomy4040038.
- Vannier MW, Staab EV, Clarke LC. 2002. Medical image archives present and future. In: Lemke HU, Inamura K, Doi K, Vannier MW, Farman AG, Reiber JHC eds. *CARS 2002 Computer Assisted Radiology and Surgery*. Berlin, Heidelberg: Springer, 565–570. DOI: 10.1007/978-3-642-56168-9_94.
- Wagner K. 1935. Endocranial Diameters and Indices. A New Instrument for Measuring Internal Diameters of the Skull. *Biometrika* 27:88–132. DOI: 10.2307/2332040.
- Weber GW, Schäfer K, Prossinger H, Gunz P, Mitteröcker P, Seidler H. 2001. Virtual Anthropology: The Digital Evolution in Anthropological Sciences. *Journal of PHYSIOLOGICAL ANTHROPOLOGY and Applied Human Science* 20:69–80. DOI: 10.2114/jpa.20.69.
- Wilkinson MD, Dumontier M, Aalbersberg IjJ, Appleton G, Axton M, Baak A, Blomberg N, Boiten J-W, da Silva Santos LB, Bourne PE, Bouwman J, Brookes AJ, Clark T, Crosas M, Dillo I, Dumon O, Edmunds S, Evelo CT, Finkers R, Gonzalez-Beltran A, Gray AJG,

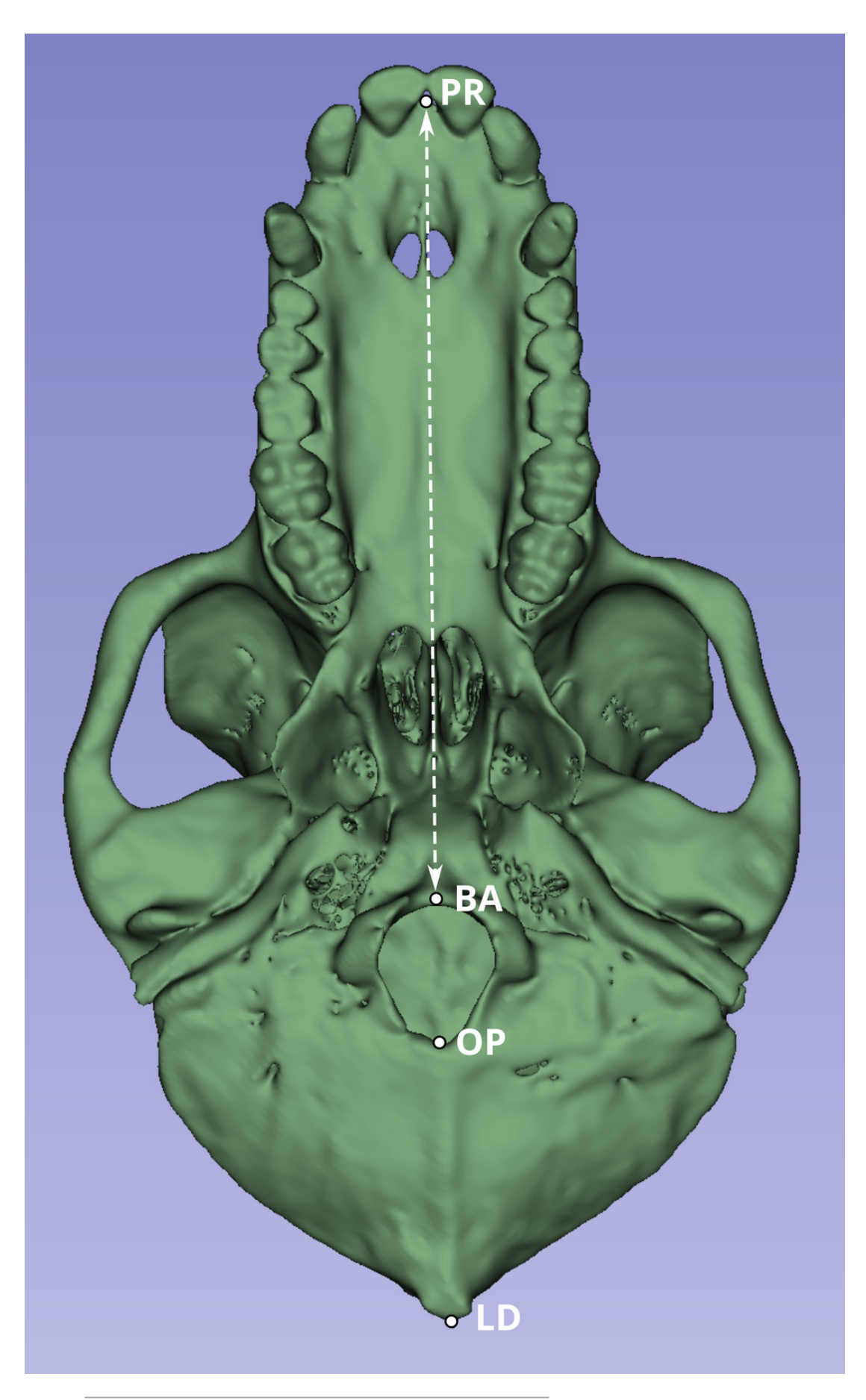


- Groth P, Goble C, Grethe JS, Heringa J, 't Hoen PAC, Hooft R, Kuhn T, Kok R, Kok J, Lusher SJ, Martone ME, Mons A, Packer AL, Persson B, Rocca-Serra P, Roos M, van Schaik R, Sansone S-A, Schultes E, Sengstag T, Slater T, Strawn G, Swertz MA, Thompson M, van der Lei J, van Mulligen E, Velterop J, Waagmeester A, Wittenburg P, Wolstencroft K, Zhao J, Mons B. 2016. The FAIR Guiding Principles for scientific data management and stewardship. *Scientific Data* 3:160018. DOI: 10.1038/sdata.2016.18.
- Willmore KE, Roseman CC, Rogers J, Richtsmeier JT, Cheverud JM. 2009. GENETIC VARIATION IN BABOON CRANIOFACIAL SEXUAL DIMORPHISM. *Evolution* 63:799–806. DOI: 10.1111/j.1558-5646.2008.00593.x.
- Wu X, Schepartz LA. 2009. Application of computed tomography in paleoanthropological research. *Progress in Natural Science* 19:913–921. DOI: 10.1016/j.pnsc.2008.10.009.
- Yu C, Qin F, Li Y, Qin Z, Norell M. 2022. CT Segmentation of Dinosaur Fossils by Deep Learning. *Frontiers in Earth Science* 9. DOI: 10.3389/feart.2021.805271.
- Yu C, Qin F, Watanabe A, Yao W, Li Y, Qin Z, Liu Y, Wang H, Jiangzuo Q, Hsiang AY, Ma C, Rayfield E, Benton MJ, Xu X. 2024. Artificial intelligence in paleontology. *Earth-Science Reviews* 252:104765. DOI: 10.1016/j.earscirev.2024.104765.
- Zhang C, Porto A, Rolfe S, Kocatulum A, Maga AM. 2022. Automated landmarking via multiple templates. *PLOS ONE* 17:e0278035. DOI: 10.1371/journal.pone.0278035.
- Zollikofer CPE, Ponce De León MS, Martin RD. 1998. Computer-assisted paleoanthropology. *Evolutionary Anthropology: Issues, News, and Reviews* 6:41–54. DOI: 10.1002/(SICI)1520-6505(1998)6:2<41::AID-EVAN2>3.0.CO;2-Z.



Inferior view of the cranium of baboon W281.

The dashed white line indicates the linear distance used to compare measurements obtained from the original skulls (using calipers and the Microscribe digitizer) with those derived from CT-based models. Anatomical landmarks are labeled as follows: PR = Prosthion, BA = Basion, OP = Opisthion, and LD = Lambda.

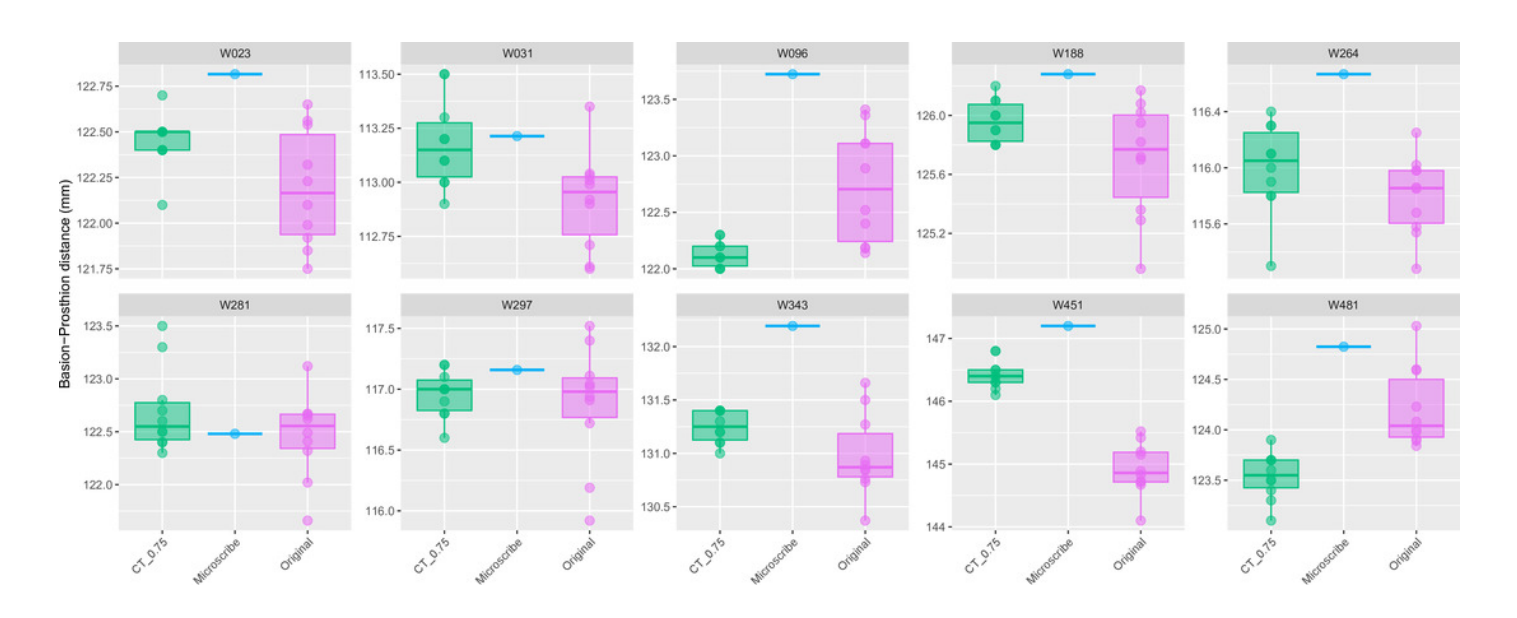


PeerJ reviewing PDF | (2025:05:119166:1:1:NEW 13 Aug 2025)



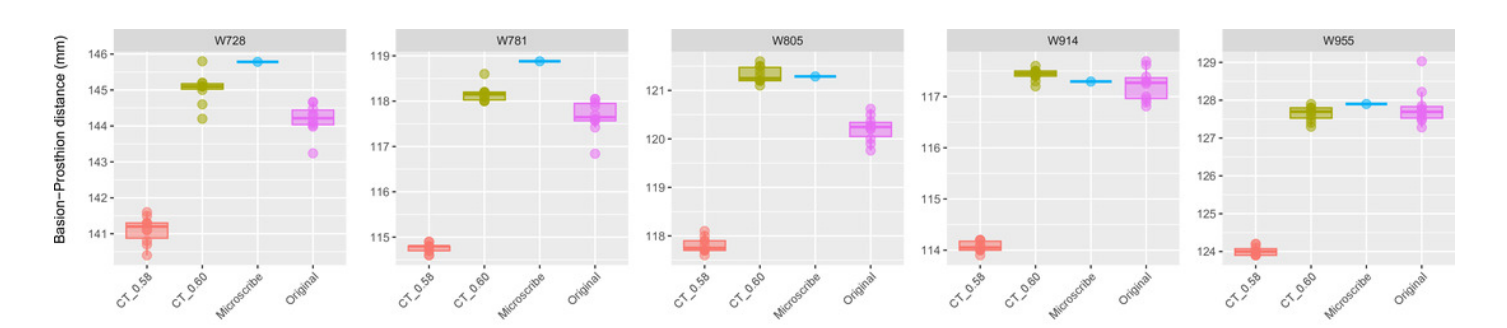
Boxplots illustrating BA-PR distances across models for crania in Group 1.

This group comprises 10 individuals randomly selected from specimens W001 to W487, all with a CT slice spacing of 0.75 mm. The CT scans for these individuals did not generate any warning messages related to slice spacing artifacts. For each individual, the BA-PR distance was measured ten times on the CT-derived model (CT_0.75), ten times on the corresponding physical skull (Original), and once using the Microscribe digitizer, as reported by Joganic et al. (2018). Notably, the range of BA-PR distances (Y-axis) spans only ~1.5 mm between minimum and maximum values. The selected specimens were: W023, W031, W096, W188, W264, W281, W297, W343, W451, and W481.



Boxplots illustrating BA-PR distances across models for crania in Group 2.

This group includes 5 individuals randomly selected from specimens W670 to W985, all with a CT slice spacing of 0.60 mm. None of the CT scans for these individuals generated warning messages related to slice spacing. For each individual, the BA-PR distance was measured ten times on the CT-derived model using the default slice spacing of 0.60 mm (CT_0.60), ten times on a model with the manually adjusted spacing of 0.58 mm (CT_0.58), ten times on the corresponding physical skull (Original), and once using the Microscribe digitizer, as reported by Joganic et al. (2018). The range of BA-PR distances (Y-axis) across all models is approximately 5 mm. The selected specimens were: W728, W781, W805, W914, and W955.



Boxplots illustrating BA-PR distances across models for crania in Group 3.

This group comprises 5 individuals randomly selected from specimens W488 to W669, all of which had a reported CT slice spacing of 0.60 mm. However, loading these scans into 3D Slicer triggered a slice spacing error, creating uncertainty as to whether the true slice spacing is 0.60 mm (as indicated by the manually entered DICOM metadata) or 0.58 mm (as automatically inferred by 3D Slicer and Amira-Avizo). For each individual, the BA-PR distance was measured ten times on the CT-derived model using the automatically loaded spacing of 0.58 mm (CT_0.58), ten times using the manually corrected spacing of 0.60 mm (CT_0.60), ten times on the corresponding physical skull (Original), and once using the Microscribe digitizer, as reported by Joganic et al. (2018). The range of BA-PR distances (Y-axis) across all models is approximately 5 mm. The selected specimens were: W489, W535, W614, W620, and W650.

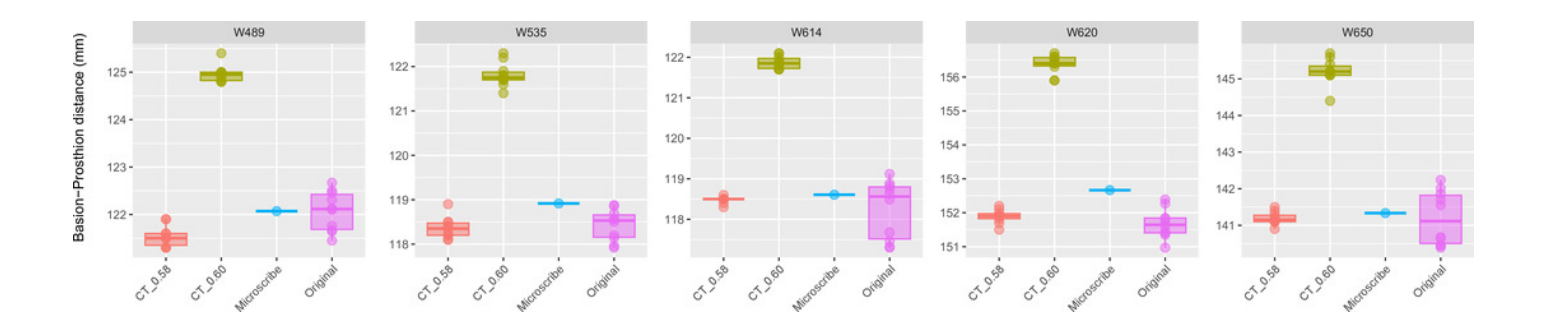




Table 1(on next page)

Pair-wise Welch's tests in each baboon skull between all the models in Group 1, Group 2, and Group 3.

Comparisons were conducted among all available models within each Group: physical skull (Original) and the CT models with 0.58, 0.60 and 0.75 mm (CT_0.58, CT_0.60 and CT_0.75, respectively). The two models that were compared and their associated sample sizes are provided in the columns labeled Model 1, Model 2, n1, and n2, respectively. The output of the Welch's test is provided in the statistic column, along with the degree of freedom (df), p-value (p), the adjusted p-value (p.adj), and the significance of the adjusted p-value (p.adj.signif). The interpretation of the significance is: ns, not significant (p > 0.05); ** (p \leq 0.05); ** (p \leq 0.001); **** (p \leq 0.001); ***** (p \leq 0.0001).



Group	WUSTL	group1	group2	n1	n2	statistic	df	р	p.adj	p.adj.signif
	W23	CT_0.75	Original	10	10	2.90	9.00	0.02	0.72	ns
	W31	CT_0.75	Original	10	10	2.26	9.00	0.05	1.00	ns
	W96	CT_0.75	Original	10	10	-3.70	9.00	0.01	0.20	ns
	W188	CT_0.75	Original	10	10	2.15	9.00	0.06	1.00	ns
	W264	CT_0.75	Original	10	10	1.15	9.00	0.28	1.00	ns
Group 1	W281	CT_0.75	Original	10	10	1.46	9.00	0.18	1.00	ns
	W297	CT_0.75	Original	10	10	0.44	9.00	0.67	1.00	ns
	W343	CT_0.75	Original	10	10	1.84	9.00	0.10	1.00	ns
	W451	CT_0.75	Original	10	10	16.31	9.00	0.00	0.00	***
	W481	CT_0.75	Original	10	10	-3.71	9.00	0.01	0.20	ns
		CT_0.58	CT_0.60	10	10	-37.64	9.00	0.00	0.00	***
	W728	CT_0.58	Original	10	10	-20.89	9.00	0.00	0.00	***
		CT_0.60	Original	10	10	4.49	9.00	0.00	0.08	ns
		CT_0.58	CT_0.60	10	10	-55.32	9.00	0.00	0.00	***
	W781	CT_0.58	Original	10	10	-29.20	9.00	0.00	0.00	***
		CT_0.60	Original	10	10	4.47	9.00	0.00	0.08	ns
	W805	CT_0.58	CT_0.60	10	10	-64.20	9.00	0.00	0.00	***
Group 2		CT_0.58	Original	10	10	-21.72	9.00	0.00	0.00	***
		CT_0.60	Original	10	10	12.59	9.00	0.00	0.00	***
	W914	CT_0.58	CT_0.60	10	10	-67.35	9.00	0.00	0.00	***
		CT_0.58	Original	10	10	-29.24	9.00	0.00	0.00	***
		CT_0.60	Original	10	10	1.86	9.00	0.10	1.00	ns
		CT_0.58	CT_0.60	10	10	-57.24	9.00	0.00	0.00	***
	W955	CT_0.58	Original	10	10	-23.43	9.00	0.00	0.00	***
		CT_0.60	Original	10	10	-0.84	9.00	0.43	1.00	ns
Group 3		CT_0.58	CT_0.60	10	10	-73.29	9.00	0.00	0.00	***
	W489	CT_0.58	Original	10	10	-3.17	9.00	0.01	0.44	ns
		CT_0.60	Original	10	10	19.76	9.00	0.00	0.00	***
		CT_0.58	CT_0.60	10	10	-57.41	9.00	0.00	0.00	***
	W535	CT_0.58	Original	10	10	-0.42	9.00	0.68	1.00	ns
		CT_0.60	Original	10	10	25.26	9.00	0.00	0.00	***
	W614	CT_0.58	CT_0.60	10	10	-83.32	9.00	0.00	0.00	***
		CT_0.58	Original	10	10	1.01	9.00	0.34	1.00	ns



		CT_0.60	Original	10	10	14.81	9.00	0.00	0.00	***
		CT_0.58	CT_0.60	10	10	-80.90	9.00	0.00	0.00	***
	W620	CT_0.58	Original	10	10	1.44	9.00	0.18	1.00	ns
		CT_0.60	Original	10	10	28.68	9.00	0.00	0.00	***
		CT_0.58	CT_0.60	10	10	-42.83	9.00	0.00	0.00	***
	W650	CT_0.58	Original	10	10	-0.03	9.00	0.98	1.00	ns
		CT_0.60	Original	10	10	18.37	9.00	0.00	0.00	***



Table 2(on next page)

Prediction intervals (upper and lower limits, confidence = 0.99) for Group 1 represented in the boxplots of Figure 2 .

The microscribe measurement for each individual is within the range of the prediction intervals from the Sample (TRUE) or (FALSE).*

* Microscribe = measurement derived from the microscribe landmark data; Sample = the different data-collection methods; CT-0.75 = measurements taken from the model of the skull created with a slice spacing of 0.75mm; Original = measurements taken from the physical skull using calipers. All measurements in mm.



_					Prediction	interval (0.99)	
	Group	WUSTL	Microscribe	ModelSa mple	Lower	Upper	Included
		W23	122.82	CT_0.75	121.94	122.96	TRUE
		W 23		Original	121.10	123.28	TRUE
		W31	113.21	CT_0.75	112.48	113.88	TRUE
		W 31		Original	112.14	113.69	TRUE
		W96	123.72	CT_0.75	121.73	122.53	FALSE
		VV 90		Original	121.02	124.44	TRUE
		W188	126.28	CT_0.75	125.47	126.45	TRUE
				Original	124.37	127.04	TRUE
	Group 1	W264 W281	116.67 122.48	CT_0.75	114.90	117.10	TRUE
				Original	114.84	116.77	TRUE
				CT_0.75	121.34	124.06	TRUE
				Original	121.10	123.83	TRUE
		W297	117.16	CT_0.75	116.31	117.61	TRUE
		VV 237	117.10	Original	115.19	118.56	TRUE
		74/3/13	7343 132.19	CT_0.75	130.74	131.76	FALSE
		W 343		Original	129.66	132.30	TRUE
		W451	147.20	CT_0.75	145.64	147.22	TRUE
				Original	143.50	146.34	FALSE
		W481	124.82	CT_0.75	122.75	124.33	FALSE
		4401		Original	122.86	125.57	TRUE



Table 3(on next page)

Prediction intervals (upper and lower limits, confidence = 0.99) for Groups 2 and 3 represented in the boxplots of Figures 3-4.

The microscribe measurement for each individual is within the range of the prediction intervals from the Sample (TRUE) or (FALSE).* * Microscribe = measurement derived from the microscribe landmark data; Sample = the different data-collection methods; CT-0.60 = measurements taken from the model of the skull created with a slice spacing of 0.60 mm; $CT_0.58 = measurements$ taken from the model of the skull created with a slice spacing of 0.58 mm; Original = measurements taken from the physical skull using calipers. All measurements in mm.



	Prediction interval (0.99)					
Group	WUSTL	Microscribe	ModelSa mple	Lower	Upper	Included
			CT_0.60	143.63	146.45	TRUE
	W728	145.78	Original	142.77	145.61	FALSE
			CT_0.58	139.83	142.39	FALSE
			CT_0.60	117.55	118.77	FALSE
	W781	118.88	Original	116.42	118.91	TRUE
			CT_0.58	114.39	115.13	FALSE
			CT_0.60	120.75	121.89	TRUE
Group 2	W805	121.29	Original	119.31	121.11	FALSE
			CT_0.58	117.27	118.35	FALSE
			CT_0.60	117.03	117.83	TRUE
	W914	117.29	Original	116.19	118.25	TRUE
			CT_0.58	113.71	114.43	FALSE
	W955	127.9	CT_0.60	126.98	128.32	TRUE
			Original	126.11	129.51	TRUE
			CT_0.58	123.6	124.42	FALSE
		122.07	CT_0.60	124.35	125.57	FALSE
	W489		Original	120.64	123.5	TRUE
			CT_0.58	120.78	122.3	TRUE
		118.92	CT_0.60	120.89	122.73	FALSE
	W535		Original	117.23	119.62	TRUE
			CT_0.58	117.54	119.18	TRUE
			CT_0.60	121.34	122.4	FALSE
Group 3	W614	118.61	Original	115.8	120.69	TRUE
			CT_0.58	118.21	118.75	TRUE
	W620	152.67	CT_0.60	155.43	157.31	FALSE
			Original	150.21	153.14	TRUE
			CT_0.58	151.22	152.56	FALSE
		141.33	CT_0.60	144	146.4	FALSE
	W650		Original	138.68	143.71	TRUE
			CT_0.58	140.6	141.78	TRUE